IEEE Sensors Letters Volume 2(3) (2017)
Sensor Applications

Sensorized facemask with moisture-sensitive RFID antenna

Giulio Maria Bianco* and Gaetano Marrocco**
Department of Civil Engineering and Computer Science Engineering, University of Tor Vergata, Roma, RM 00133, Italy
** Graduate Student Member, IEEE*
*** Member, IEEE*

Abstract—Due to the ongoing COVID-19 pandemic, the use of Filtering Facepiece Respirators (FFRs) is increasingly widespread. Since the masks' wetness can reduce its filtering capabilities, the World Health Organization advises to replace the FFRs if they become too damp, but, currently, there is no practical way to monitor the masks' wetness. A low-cost moisture sensor placed inside the FFRs could discriminate a slightly damp mask from a wet one which must be replaced. In this paper, a RadioFrequency Identification (RFID) tag exploiting an auto-tuning microchip for humidity sensing is designed and tested during an ordinary working day and a physical exercise. The tag returns about 1 unit of the digital metric every 3 milligrams of water generated by breathing and sweating, and it can identify excessively wet masks from commonly used ones.

Index Terms— Auto-tuning, filtering facepiece respirators, personal protective equipment, radiofrequency identification, sensor applications, wearable antennas.

I. INTRODUCTION

Face protections, like the Filtering Facepiece Respirators (FFRs), can significantly reduce the risk of infection caused by respiratory pathogens [1]. Because of the ongoing COVID-19 pandemic, the World Health Organization advises for the universal masking in health facilities, and the FFRs should be replaced as soon as they become damp [1]. However, such widespread use of masks can cause supply shortages, and their use must be optimized. As recommended by the USA National Institute for Occupational Safety and Health [2], the current practice is not to wear the same mask twice and replace it after a maximum of eight hours of continuous use. Indeed, moisture produced by breath causes an increase of the Relative Humidity (RH) of the interior microclimate and some condensation on the internal surface of the FFR. This was reported to decrease the filtering effect [3, 4]. Moreover, the moisture in the FFR's deadspace (i.e. the volume between the mask and face) is linked to user discomfort [5].

To discriminate a dry or slightly damp mask from a wet one that needs to be replaced, a low-cost moisture sensor could be placed inside the mask to monitor its effectiveness. The moisture sensing could also be useful to optimize the decontamination cycles of the FFRs [6]. FFRs equipped with RadioFrequency Identification (RFID) tags have been recently proposed for managing the medical supply chains [7]. RFID sensor-tags for humidity can exploit the antenna performance variations, such as frequency shift [8] or power collected by the IC [9]. The price to pay for sensing is a degradation of the read-range as humidity and moisture increase. A different approach considers instead a dedicated external sensor connected to the tag [10]. Although the communication performance is preserved, this solution involves higher complexity and cost, making the application into a cheap FFR rather impractical.

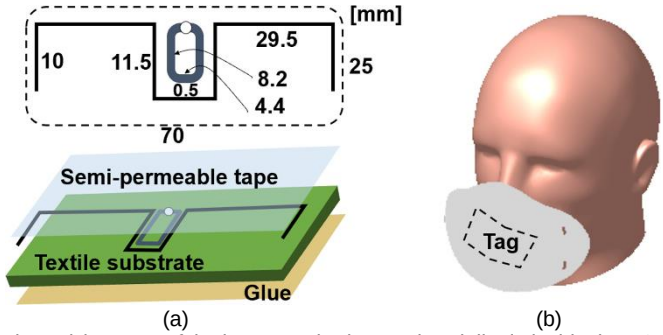

Fig. 1. (a) Layout of the loop-matched meandered dipole inside the N95 mask and exploded view of the tag. The loop is an aluminum 35 μm thick trace whereas the dipole is made of a thin copper wire (diameter 40 μm). (b) Simplified anthropomorphic numerical phantom of the head used for the electromagnetic simulations, and tag's placement on the internal surface of the N95 mask.

This paper proposes a facemask-integrated moisture sensor that only relies on a thin-wire antenna and an auto-tuning [11] Integrated Circuit (IC) so that this advanced sensing device can be low-cost and avoid degradations of the link range. The antenna is fixed onto a hygroscopic and hydrophilic fiber inside an N95 FFR. The tag's electromagnetic performance is optimized through numerical simulations comprising a model of the head and an N95 facemask. Hence, prototypes are manufactured and experimented in both regular and stressful activities.

II. SENSING BY AUTO-TUNING ICs

The RFID-based moisture sensor exploits the unique features of a new family of RFID ICs with an auto-tuning capability. They can dynamically change their internal impedance to maximize the power collected by the IC and compensate for a possible impedance mismatch with the antenna due to changes in the boundary conditions

Corresponding author: G. M. Bianco (Giulio.Maria.Bianco@uniroma2.it)

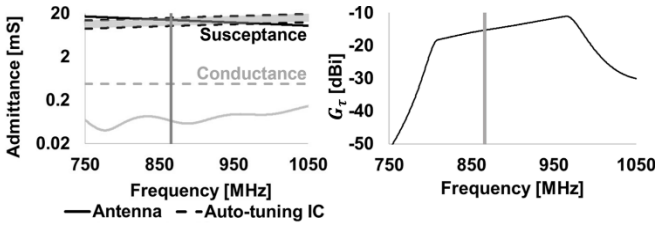

(a) (b)

Fig. 2. Simulated performance of the tag's antenna. The EU unlicensed 865-867 MHz band is highlighted in grey. (a) Admittances of the tag's antenna and the IC. The shadowed region indicates the dynamic range of the susceptance that the auto-tuning IC can match. (b) Realized gain of the sensor-tag along the nasal septum direction

[11], here the amount ψ of moisture on the facemask. Indeed, the mismatch is related to the absorbed moisture, which changes the substrate's permittivity locally and disturbs the antenna. The analog front-end of an auto-tuning IC includes a varactor device that can be modelled as a resistance parallel to a variable capacitance [11]. The capacitance, in turn, can be considered as a switchable ladder of N identical capacitors having a total capacitance C_{IC}. C_{IC} spans from a minimum C_{min} to a maximum value with incremental steps C_0 according to the law $C_{IC}(n) = C_{min} + nC_0$ where n is the number of connected equivalent capacitors. The auto-tuning feature can be exploited for the indirect sensing of the status ψ of the facemask, which is related to the internal IC capacitance by the equation [12]:

$$|2\pi f C_{IC}(n) + B_A(\psi)| = 0 \qquad (1)$$

where f is the frequency and B_A is the susceptance of the tag's antenna. Equation (1) holds for $N_{min} \le n \le N_{max}$, whereas outside of this range, there is saturation [13]. Auto-tuning ICs return a digital metric, hereafter denoted as *Sensor Code* (*SC*), which is directly proportional to n by inverting (1) and accounting for the saturation:

$$SC(\psi) = N_{min} + nint\left[-\frac{1}{C_0}\left(C_{min} + \frac{B_A(\psi)}{2\pi f}\right)\right] \qquad (2)$$

where *nint*(x) is the nearest integer to x. User-specific baselines can be removed through calibration with respect to the Sensor Code SC_0 returned just after the placement on the face, thus obtaining a *Differential Sensor Code* [14], $\Delta SC = SC_{measured} - SC_0$. Since B_A is unknown in real use, the relationship $SC(\psi)$ must be determined through an experimental calibration curve, as shown in the following.

III. THE TEXTILE MOISTURE SENSOR-TAG

The sensitive substrate to collect the moisture produced by the breath is an inexpensive twill woven fabric (50% cotton, 50% nylon) of size 70 mm × 25 mm × 1 mm. The textile has hydrophilic and hygroscopic properties [15] and absorbs liquid due to both the RH and condensation. The twill woven substrate hosts a symmetric loop-matched [16] meandered dipole (Fig. 1(a)) that is connected to an Axzon S3 Magnus auto-tuning IC [13] with parameters $N_{min} = 80$,

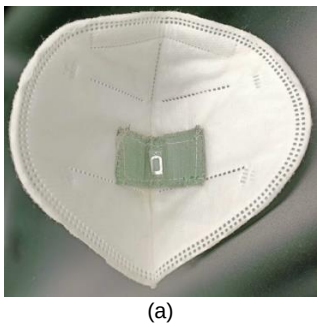

(a) (b)

Fig. 3. (a) Prototype of a facemask tag glued inside an N95 FFR. (b) Zoomed-in view of one tag prototype.

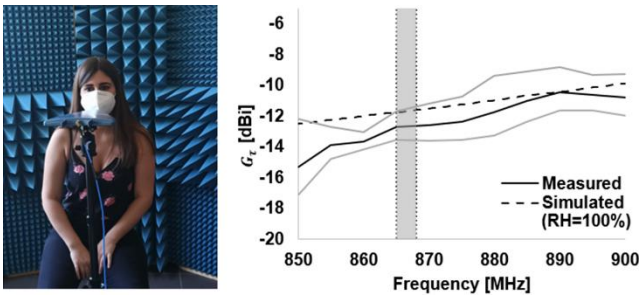

(a) (b)

Fig. 4. Measurement of the electromagnetic performance of the tagged FFRs. (a) Arrangement in a semi-anechoic space and (b) average measured and simulated (RH=100%) realized gain over the three prototypes each worn by a different volunteer. Grey lines indicate the average measured values plus and minus the standard deviations**.** The EU unlicensed 865-867 MHz band is highlighted in grey.

$N_{max} = 420$, $G_{IC} = 0.482$ mS , $C_{min} = 1.9$ pF, $C_{max} = 2.9$ pF and power threshold $p_{IC} = -16.6$ dBm. Accordingly, the resulting IC susceptance can retune in the range 10.3 mS $\le B_{IC} \le$ 15.8 mS at 866 MHz, and the corresponding middle-range impedance is $Z_{IC} = 2.8 - j76.1\ \Omega$. The resulting sensor-tag is placed in the core region of the FFR (Fig. 1(b)), which is expected to be the wettest portion of the internal surface [17]. The added surface covers a small part of the mask, and the only expected consequence on the FFR's effectiveness is a slightly improved filtering capability.

The geometrical parameters of the antenna were optimized through numerical simulations (by CST Microwave Studio 2018) assuming it is attached on an N95 FFR made of polypropylene (ε = 2.2, tanδ = 0.002 [18]). Simulations accounted for the human head by an anthropomorphic homogeneous numerical phantom[1] (ε = 42.7, σ = 0.99 S/m [19]). The final antenna form factor constrains the input susceptance inside the IC's tuning range (the shadowed region in Fig. 2(a)) for 830 MHz $\le f \le$ 980 MHz. The achieved realized gain is higher than $G_{\tau,min} = -15$ dBi along the direction of the nasal septum (Fig. 2(b)). Thanks to the auto-tune property of the IC, G_τ exhibits the typical nearly flat profile over a broad band. By assuming the reader emits not less than 22 dBm (low-cost handheld device) a read distance longer than 40 cm is expected. In this way, an operator with arms' length longer than 60 cm [20] could monitor a third-person facemask's status while keeping a safety droplet-free distance of at least 1 m [1]. Moreover, as previously demonstrated in [10], this

[1] Model available at https://grabcad.com/library/helmet-184 and https://grabcad.com/library/n95-mask-covid-19-1.

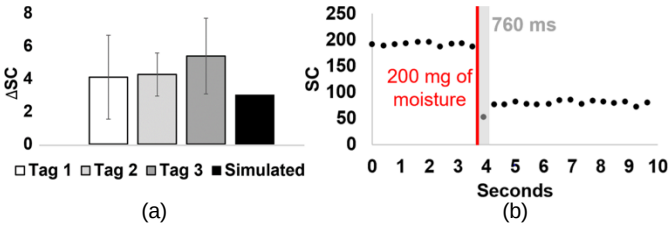

(a) (b)

Fig. 5. (a) Measured and simulated ΔSC after 10 minutes in the climatic chamber. (b) Step response of the tagged facemask when 200 mg of a physiologic solution are sprayed over its interior surface.

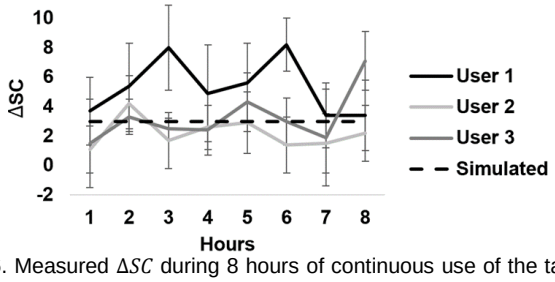

Fig. 6. Measured ΔSC during 8 hours of continuous use of the tagged facemasks during everyday activities, compared with the simulated value.

arrangement will be fully compliant with Specific Absorption Rate (SAR) regulations.

IV. PROTOTYPES AND EXPERIMENTATION

A. Test in Controlled Conditions

Some tag's prototypes were manufactured by fixing the dipole, made of a thin copper wire, onto the fabric substrate through a semi-permeable, transparent polyvinyl chloride film (Tegaderm, thickness 25 μm). The boundaries of the resulting tags were then glued inside N95 FFRs (Fig. 3). Three volunteers wore a prototype each, and the realized gain was measured in the direction of the nasal septum by through a Voyantic Tagformance Pro station. The measured data (Fig. 4) compare well with the simulations, and the average difference is just 1 dB. The three prototypes were then placed inside a Binder MKF 56 climatic chamber to perform a test on the Sensor Codes when the ambient humidity is firstly kept at 10%, then raised to 100% and kept for 10 minutes. The ΔSC was measured by ensuring a fixed value of on-chip Received Signal Strength Indicator (set to 15 units) to avoid possible nonlinearities of the self-tuning mechanism [11]. For comparison, RH values were accounted for in the simulations by considering two permittivity values of the tag substrate (ε=2 at RH=10% and ε=2.4 at RH=100%) [15]. The measured ΔSC is slightly higher than the simulated one (Fig. 5(a)), probably due to the approximated model of auto-tuning ICs and the effects of condensation of moisture on the tag, not accounted for in the simulations. The sensor's response time is evaluated by stimulating the step response through a sharp exposure of 200 mg of physiologic solution sprayed inside a sensorized dry facemask (Fig.5(b)). The Sensor Code was continuously measured before, during and after the event. The discontinuity was nearly instantaneously detected with just 0.8 s settling time, corresponding to a single sample.

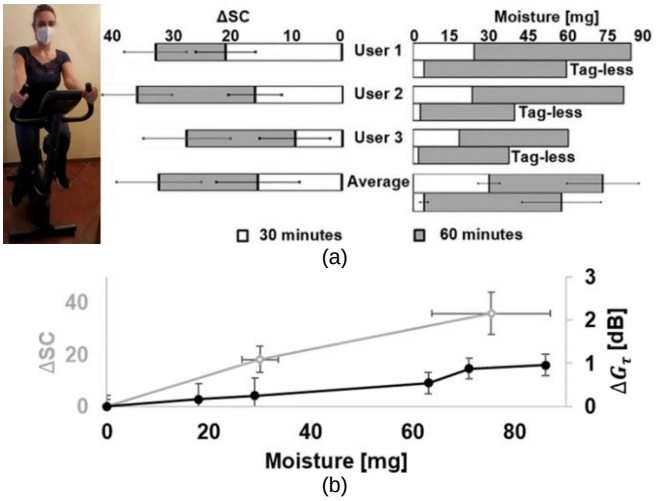

(a)

(b)

Fig. 7. (a) Measured ΔSC after 30 and 60 minutes of physical exercise with a stationary bike and the corresponding measured water moisture collected by the tagged and tag-less FFRs. (b) Measured ΔG_τ and ΔSC vs. the moisture collected by the mask.

B. Experimentation in Everyday Conditions

The volunteers wore the three N95 FFRs for one 8-hours working shift. They interacted with computers and performed several non-challenging physical tasks, like walking to a shop. The FFRs were occasionally removed for less than ten consecutive minutes, and the ΔSC was always checked before and after the removal to be sure that the measurements had not been affected. Three measurements per hour were performed by using a Caen qID mini handheld reader. The resulting ΔSCs (Fig. 6) fluctuated in the (−2, 10) range depending on the environment and the performed tasks. In particular, there is a cyclic profile with a 3-hours periodicity in the three cases that is probably due to the balance between cyclic generation and evaporation of the condensed moisture inside the FFRs' deadspaces. Consequently, the effective variation of the SC in regular use is modest and does not permit to discriminate relevant events. A more significant behavior was instead appreciated in stressful conditions, as described next.

C. User under Physical Stress

The volunteers were asked to perform an intense physical exercise while continuously wearing the FFRs. They had to ride a stationary bike for an hour (maximum resistance, speed 16 km/h, indoor temperature 27 °C). The test was repeated with regular masks without the RFID sensors to evaluate the absorption capability of the sensor's substrate. In both tests, the masks were weighted after 30 minutes and then after 60 minutes of exercise. The weight increments of the tag-less N95s, as measured during the second session, are consistent with values reported in [17, 21, 22]. In comparison with the tag-less masks (Fig. 7(a)), the properties of the tag substrate allowed the sensorized masks to collect an additional quantity of moisture (in average, an extra 27% of water after 1 hour of physical exercise), especially during the first 30 minutes. Therefore, the sensitivity to breath is amplified, and the capability of predictive monitoring of the mask status is improved. Correspondingly, the measured ΔSCs are up to four times higher than in the previous experiment involving a weaker

activity. Values look correlated with the weight of absorbed moisture, as shown in Fig. 7(b). There is a detectable difference between the two states which are well identified in all the cases. The $\Delta SC(\psi)$ profile (averaged over the three users) is nearly linear, and the estimated sensitivity is $S(\psi) \approx 0.35$ units per mg of moisture. Finally, the reduction of realized gain (ΔG_τ) vs. the condensed moisture during the exercise was of the order of just 0.1 dB per 10 mg. The maximum degradation in the extreme condition is 1 dB that converts in a 10% reduction of the read distance, at most. Accordingly, the electromagnetic performance stays almost stable during the increasing humidification of the mask.

V. CONCLUSION

A textile integrated moisture sensor-tag based on an auto-tuning RFID IC was designed for application onto an N95 facemask and tested by volunteers in realistic conditions. When the mask is worn, an initial calibration is required to reduce the user variability of the response. Afterwards, tags discriminated the use of the FFRs during an ordinary working day ($\Delta SC \leq 10$) from a more demanding physical activity ($\Delta SC \geq 15$), which could resemble a caregiver's hectic day in a COVID-19 hospital where the device's ageing accelerates. Hence, the sensor could help to identify excessively wet FFRs to be replaced. With the current performance, qualitative information can be retrieved. However, since the available dynamic range of the Sensor Code was only partially used, there is a margin to improve the sensitivity by further optimizing the antenna layout. It is finally worth mentioning that the employed IC also provides temperature measurements that could be merged with the moisture information to achieve more accurate predictions of the mask's ageing and even produce data on the user's respiration, fever rise and lung status [23]. These potentialities will be investigated in future works.

ACKNOWLEDGMENT

The authors thank the B.Sc. enrolled in the academic year 2020 at the Tor Vergata University of Rome (M.Sc. in Medical Engineering course) who actively contributed to the research: Aru, Luisa; De Angelis, Ludovica; Diamanti, Arianna; Fontana, Elisa; Gagliardi, Miriam; Naccarata, Federica; Salvati, Veronica; Tocci, Tiziana; Veltro, Giulia.

REFERENCES

[1] World Health Organization, "Advice on the use of masks in the context of COVID-19," Rep. no. WHO/2019-nCov/IPC_Masks/2020.4, June 5, 2020. Accessed: Nov. 4, 2020. [Online]. Available: https://www.who.int/publications/i/item/advice-on-the-use-of-masks-in-the-community-duringhome-care-and-in-healthcare-settings-in-the-context-of-the-novel-coronavirus-(2019-ncov)-outbreak

[2] National Institute for Occupational Safety and Health, "Recommended Guidance for Extended Use and Limited Reuse of N95 Filtering Facepiece Respirators in Healthcare Settings", Mar. 27, 2020. Accessed: Nov. 4, 2020 [Online]. Available: https://www.cdc.gov/niosh/topics/hcwcontrols/recommendedguidanceextuse.html

[3] S. Gao *et al*., "Performance of N95 FFRs against combustion and NaCl aerosols in dry and moderately humid air: manikin-based study," *Ann. Occup. Hyg*., vol. 60, no. 6, pp. 748–760, Apr. 2016.

[4] A. Pacitto *et al*., "Effectiveness of commercial face masks to reduce personal PM exposure," *Sci. Total Environ.*, vol. 650, no. 1, pp. 1582-1590, Feb. 2019.

[5] R. J. Roberge, J. Kim and S. Benson, "N95 filtering facepiece respirator deadspace temperature and humidity," *J. Occup. Environ. Hyg.*, vol. 9, no. 3, pp. 166-171, Mar. 2012.

[6] A. Schwarty *et al.*, "Decontamination and reuse of N95 respirators with hydrogen peroxide vapor to address worldwide personal protective equipment shortages during the SARS-CoV-2 (COVID-19) pandemic," *J. ABSA Int.*, vol. 25, no. 2, pp. 67-70, June 2020.

[7] H. Chan, T. Choi, C. Hui and S. Ng, "Quick response healthcare apparel supply chains: value of RFID and coordination," *IEEE Trans. Syst., Man, Cybern. Syst.*, vol. 45, no. 6, pp. 887-900, June 2015.

[8] E. M. Amin, M. S. Bhuiyan, N. C. Karmakar and B. Winther-Jensen, "Development of a low cost printable chipless RFID humidity sensor," *IEEE Sensors J.*, vol. 14, no. 1, pp. 140-149, Jan. 2014.

[9] J. Virtanen, L. Ukkonen, T. Bjorninen, A. Z. Elsherbeni and L. Sydänheimo, "Inkjet-printed humidity sensor for passive UHF RFID systems," *IEEE Trans. Instrum. Meas.*, vol. 60, no. 8, pp. 2768-2777, Aug. 2011.

[10] M. C. Caccami, M. Y. S. Mulla, C. Occhiuzzi, C. Di Natale and G. Marrocco, "Design and experimentation of a batteryless on-skin RFID graphene-oxide sensor for the monitoring and discrimination of breath anomalies," *IEEE Sensors J.*, vol. 18, no. 21, pp. 8893-8901, Nov. 2018.

[11] M. C. Caccami and G. Marrocco, "Electromagnetic modeling of self-tuning RFID sensor antennas in linear and nonlinear regimes," *IEEE Trans. Antennas Propag.*, vol. 66, no. 6, pp. 2779-2787, June 2018.

[12] G. M. Bianco and G. Marrocco, "Fingertip self-tuning RFID antennas for the discrimination of dielectric objects," in *Proc. 13th Eur. Conf. Antennas Propag.*, Krakow, Poland, Mar. 15-20 2019, pp. 1-4.

[13] G. M. Bianco, S. Amendola and G. Marrocco, "Near-field constrained design for self-tuning UHF-RFID antennas," *IEEE Trans. Antennas Propag*, vol. 68, no. 10, pp. 6906-6911, Oct. 2020.

[14] G. M. Bianco, C. Vivarelli, S. Amendola and G. Marrocco, "Experimentation and calibration of near-field UHF epidermal communication for emerging tactile internet," in *Proc. 5th Int. Conf. Smart Sustain. Technol.*, Split, Croatia, Sept. 23-26 2020, pp. 1-4.

[15] C. Hertleer, "Design of planar antennas based on textile materials," Ph.D. dissertation, Dept. Mate., Textiles Chem. Eng., Univ. Ghent, Ghent, Belgium, 2009. [Online]. Available: https://www.researchgate.net/publication/292612193_Design_of_planar_antennas_based_on_textile_materials

[16] G. Marrocco, "The art of UHF RFID antenna design: impedance-matching and size-reduction techniques," *IEEE Antennas Propag. Mag.*, vol. 50, no. 1, pp. 66-79, Feb. 2008.

[17] Q. Yang *et al*., "Study of the micro-climate and bacterial distribution in the deadspace of N95 filtering face respirators," *Scientific Rep.*, vol. 8, no. 1, Nov. 2018, Art. no. 17382.

[18] J. Hu, L. Zhang, Z. Dang and D. Wang, "Improved dielectric properties of polypropylene-based nanocomposites via co-filling with zinc oxide and barium titanate," *Composites Sci. Technol.*, vol. 148, pp. 20-26, Aug. 2017, doi: 10.1016/j.compscitech.2017.05.009.

[19] *IEEE Recommended Practice for Determining the Peak Spatial-Average Specific Absorption Rate (SAR) in the Human Head from Wireless Communications Devices: Measurement Techniques*, IEEE 1528-2013, IEEE Standards Association, Sept. 2013. [Online]. Available: https://standards.ieee.org/standard/1528-2013.html

[20] C. C. Gordon *et al*., "1988 Anthropometric survey of U.S. personnel: summary statistics interim report," U.S. Army Res., Natick, MA, USA, Rep. Natick/TR-89/027, Mar. 1989. Accessed: 27 Jan. 2021. [Online]. Available: https://apps.dtic.mil/dtic/tr/fulltext/u2/a209600.pdf

[21] R. J. Roberge, A. Coca, W. J. Williams, A. J. Palmiero and J. B. Powell, "Surgical mask placement over N95 filtering facepiece respirators: physiological effects on healthcare workers," *Respirology*, vol. 15, no. 3, pp. 516-521, Apr. 2010.

[22] R. J. Roberge. E. Bayer, J. B. Powell, A. Coca, M. R. Roberge and S. M. Benson, "Effect of exhaled moisture on breathing resistance of N95 filtering facepiece respirators," *Ann. Occup. Hyg.*, vol. 54, no. 6, pp. 671–677, Aug. 2010.

[23] J. W. Cherrie, S. Wang, W. Mieller, C. Wendelboe-Nelson and M. Loh, "In-mask temperature and humidity can validate respirator weartime and indicate lung health status," *J. Expo. Sci. Environ. Epidemiol.*, vol. 29, pp. 578–583, July 2019, doi: 10.1038/s41370-018-0089-y